

The local limit of global gyrokinetic simulations

J. Candy^{a)} and R. E. Waltz

General Atomics, P.O. Box 85608, San Diego, California 92186

W. Dorland

University of Maryland, College Park, Maryland

(Received 11 December 2003; accepted 11 February 2004; published online 14 April 2004)

Global gyrokinetic simulations of turbulence include physical effects that are not retained in local flux-tube simulations. Nevertheless, in the limit of sufficiently small ρ_* (gyroradius compared to system size) it is expected that a local simulation should agree with a global one (at the local simulation radius) since all effects that are dropped in the local simulations are expected to vanish as $\rho_* \rightarrow 0$. In this Letter, global simulations of a well-established test case are indeed shown to recover the flux-tube limit at each radius. © 2004 American Institute of Physics.

[DOI: 10.1063/1.1695358]

The purpose of this Letter is to clarify the connection between local and global gyrokinetic (GK) turbulence simulations. In previous work¹ using the GYRO code,² a study of the mechanisms by which transport scaling can be degraded from gyro-Bohm to Bohm, or to worse than Bohm, was made for ion temperature gradient (ITG) turbulence with adiabatic electrons. The critical role played by equilibrium profile shearing, particularly in cases near marginal stability, was discussed. A recurring theme in Ref. 1 was that the value of χ_i observed in a global simulation with sufficiently small value of ρ_* is the same as that found in the corresponding local (flux-tube) simulation. Here, $\rho_* \doteq \rho_s/a$ with $\rho_s \doteq c_s/\Omega_{ci}$ the ion-sound gyroradius, $c_s = \sqrt{T_e/m_i}$ the sound speed, and Ω_{ci} the ion gyrofrequency.

At about the same time, Lin *et al.*³ reported work on the size scaling of turbulent transport using a different code (GTC) and with a specific set of equilibrium profiles. Unlike GYRO, which uses an Eulerian discretization scheme, the GTC code uses the popular particle-in-cell (PIC) method to solve the GK equations. A discussion of the relative merits of each scheme is beyond the scope of the present paper and can be found elsewhere.^{4,5} Suffice it to say that because the two codes use radically different numerical methods, they are susceptible to radically different types of discretization error. In the study reported in Ref. 3, adiabatic electron dynamics and finite-aspect-ratio toroidal geometry were considered. A parameter scan was given for $1/\rho_*$ in the range $125 \leq 1/\rho_* \leq 1000$. The overarching result was to show that “the local transport coefficient exhibits a gradual transition from a Bohm-type scaling for devices sizes corresponding to present-day tokamak experiments to a gyro-Bohm scaling for future larger devices.” We remark that the scenario studied in Ref. 3 was constructed so as to match the DIII-D Cyclone Base Case at $r/a = 0.5$.⁶ However, the results in Ref. 3 showed that at $1/\rho_* = 1000$ the asymptotic value of the transport coefficient was $\chi_i \approx 3.4\chi_{GB}$, about 80% larger than the well-established local value of Dimits: $\chi_i \approx 1.9\chi_{GB}$ (see

LLNL GK result in Ref. 6). Here, $\chi_{GB} \doteq \rho_s^2 c_s/a$ defines the gyro-Bohm normalization. Note that Ref. 6 used a different normalization, $\chi_{Dimits} \doteq \rho_s^2 c_s/L_n$, such that $\chi_{GB} = 1.25\chi_{Dimits}$. This discrepancy was mentioned and attributed to finite-aspect-ratio effects in Ref. 3, which were later removed in Ref. 7, giving an asymptotic result at least as large as $\chi_i \approx 2.6\chi_{GB}$. This result is closer to, but still 35% higher than, the accepted value. The Dimits value, which is in close agreement with the GYRO Eulerian calculation, was obtained using a flux-tube GK-PIC code. This implies that the source of the GTC discrepancy cannot be based solely on choice of algorithm.

In an effort to understand these results, we made an exhaustive study of the GTC ρ_* -scan using GYRO. A variety of resolution tests and sensitivity studies were carried out in an effort to find some effect which would increase the transport to levels consistent with Ref. 7. In the end, our results repeatedly showed what we expected all along: that global simulation results approach the flux-tube limit (with corresponding gyro-Bohm scaling), and do so at a system size characteristic of medium-size tokamaks (DIII-D L-mode plasmas have $1/\rho_* \approx 300$). As an added consistency check, we have also verified that the small- ρ_* GYRO results agree with a series of simulations from the flux-tube Eulerian code GS2,⁸ as will be shown later.

The generally unstated assumption in most simulation papers is that quoted values of χ_i have reached a statistical steady-state, and are adequately converged with respect to time-step and grid resolution. It is quite impractical to prove convergence for every case by running highly overresolved simulations. In practice this is only done for a few cases, and judgments based on past experience are made for most cases. All GYRO cases reported in this paper used 128 points in velocity space (8 pitch angles, 8 energies, and 2 signs of velocity), and radial grid spacing $\Delta r = \rho_s$. An adaptive long-wavelength source is also used to prevent profile relaxation, as detailed in Ref. 1. Because of the spectral decomposition in the toroidal direction, GYRO can efficiently resolve cases at arbitrarily small ρ_* by choosing $\Delta n > 1$ (thereby simulat-

^{a)}URL: <http://web.gat.com/comp/parallel>

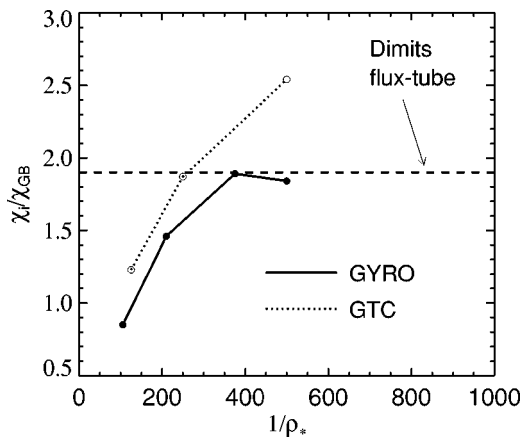


FIG. 1. Comparison of GYRO and GTC-IAEA results for the global scenario of Sec. III, Ref. 7. The dashed horizontal line shows the flux-tube result of Dimits (Ref. 6), which is an accepted benchmark value. All GYRO points correspond to the radius $r/a=0.5$ and are numerically averaged over the interval $400 \leq (c_s/a)t \leq 900$. GTC data were numerically averaged over the interval $200 \leq (c_s/a)t \leq 500$ (note that $c_s = v_i$).

ing a toroidal wedge of width $2\pi/\Delta n$). Here, n is the toroidal mode number. In this Letter, we used between 16 and 64 toroidal modes, as needed, although our experience is that rarely are cases encountered for which more than 32 modes are required.

With regard to the time domain, it is problematic in practice to determine whether or not a very expensive case is really in a stationary state having no trend, simply because it costs twice as much to run twice as long. In the end, there is no practical way to avoid the need for “good judgment.” A key advantage of Eulerian codes, however, is the absence of noise build-up with run time, so that the existence of a stationary state can in principle be demonstrated. Inexpensive GYRO cases have been run to time scales ten times longer than those shown here with no indication of up- or down-trends in χ_i . Furthermore, in GYRO, we have verified the neutral linear stability of the $n=0$ radial modes (zonal flows) for very long times. This is an important and strenuous test for cases with large radial domain size.

We summarize the present state of comparison between GYRO and published GTC results in Fig. 1, which shows the gyro-Bohm-normalized ion thermal diffusivity, χ_i/χ_{GB} versus $1/\rho_*$ for each code. In Ref. 7 it is argued that the difference between the gyro-Bohm limit (horizontal line) and the GTC value is a consequence of nonperiodic boundary conditions, large radial domain size and radial variation of ω_* , q , s , and r/R used in the latter calculation. However, our results show that this explanation is not valid, since GYRO includes all these aforementioned effects yet agrees with the local result. There is also the unexplored possibility that the different sources in GTC and GYRO, which act to maintain the equilibrium profiles, give rise to the difference.

While the nonspecialist would probably assume that global gyrokinetic codes would readily accept as input arbitrary temperature and density profiles, this is not generally the case. There are certain assumptions of nonphysical origin which are routinely made in global codes in order to facilitate simulations. One of the more common and problematic

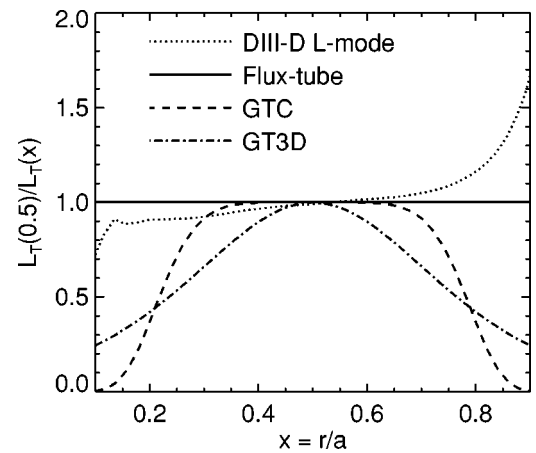


FIG. 2. Comparison of a DIII-D experimental logarithmic temperature gradient profile (dotted curve) with those assumed in various types of numerical simulations. The GT3D (dotted-dashed) (Refs. 12, 13) and GTC (dashed) (Refs. 3, 7, 10, 11) curves illustrate the peaked form routinely employed in global GK-PIC codes. The flux-tube (solid) curve shows the constant value used in flux-tube simulations.

of these is the radial shape of the inverse-temperature-gradient scale-length profile, $1/L_T(r) \doteq -(1/T)(dT/dr)$. The customary setup^{3,9-13} for a global GK-PIC simulation is to place the largest instability drive at the center of the simulation domain, with vanishing drive near the simulation boundaries. In typical L-mode and H-mode discharges, however, $1/L_T$ does not show this trend but rather tends to increase from core to edge, rising sharply near the edge. This is shown in Fig. 2 for a DIII-D L-mode discharge (# 101381) we have simulated elsewhere¹⁴ using full-physics and actual experimental profiles in real shaped geometry. Flux-tube codes, on the contrary, can only treat flat profiles across the radial simulation domain (in practice, a flux-tube simulation describes transport over a small fraction of the minor radius). One obvious feature of the GK-PIC gradient profiles shown in Fig. 2 is the central peaking that is present neither in experiments nor in flux-tube simulations. More specifically, the GTC *hump* gradient profile has no shearing in the center, but huge shearing in the inner and outer 1/4th of the radial domain.

These artificial features may be responsible, at least in part, for the difficulty some GK-PIC codes face in recovering flux-tube results—and gyroBohm scaling—as $\rho_* \rightarrow 0$. Specifically, the greater the profile shearing, the smaller the required ρ_* to approach the local result, as demonstrated in Ref. 1. GYRO was designed with these considerations in mind, and uses a boundary interface algorithm which can accommodate any equilibrium profile shape: flat, peaked, or experimental. In the general case, GYRO can read the equilibrium profiles directly from an experimental dataset over the entire simulation radius.

To quantitatively demonstrate the effect of profile shear on transport scaling for this Cyclone case, we start by writing the form of the *humped* gradient profile as used in Refs. 3 and 7 as

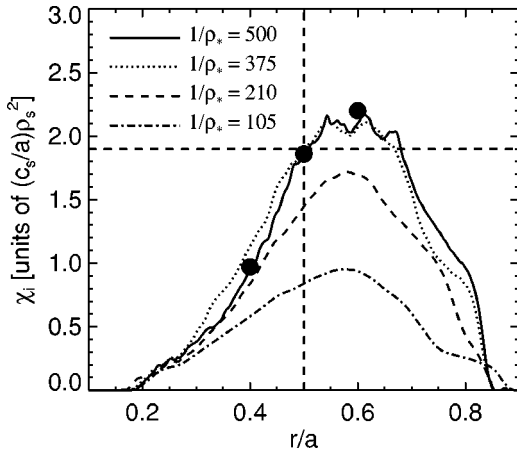


FIG. 3. Curves show radial profile of χ_i averaged over the time interval $400 \leq (c_s/a)t \leq 900$, as computed by GYRO. Solid dots show results of three separate GS2 flux-tube simulations.

$$\frac{dT}{dr} = \left(\frac{dT}{dr} \right)_0 \exp\{-[(r/a - 0.5)/0.3]^6\}. \quad (1)$$

While the temperature gradient above is radially varying, the temperature itself is artificially held constant: $T(r) = T_0$. The maximum value of the temperature gradient is taken to match the Cyclone Base Case value of $R_0/L_{T,0} = -(R_0/T_0)(dT/dr)_0 = 6.9$. These profiles were used by both codes in Fig. 1, and as we have already noted, introduce a region of strong profile shearing and low drive in the inner and outer 1/4th of the radial domain. Corresponding to the four points on the GYRO curve in Fig. 1 are the radial χ_i profiles illustrated in Fig. 3. As an independent check on these results, the flux-tube GS2 code was run at $r/a = 0.4, 0.5, \text{ and } 0.6$, with the results shown as large dots in Fig. 3. The close agreement between GYRO global results and GS2 local results for this case supports the conclusion that (i) both codes are operating correctly, and (ii) local and global turbulence codes should agree for sufficiently small ρ_* . Now, if we rerun the same case, only replacing the profile of Eq. (1) with a *ramped* temperature gradient of the form

$$\frac{dT}{dr} = \left(\frac{dT}{dr} \right)_0 [1 + 0.3(r/a - 0.5)], \quad (2)$$

we observe a transition to gyro-Bohm scaling at a much smaller system size (larger ρ_*). This result is summarized in Fig. 4.

Verification of numerical convergence for gyrokinetic codes is an extraordinarily challenging issue. Because the simulation cost rises rapidly as the resolution is increased, convergence studies are rarely exhaustive. In connection with this, we have noticed that early-time estimates of χ_i are affected by transient phenomena and tend to overestimate the true steady-state value. For this reason, all GYRO simulations in the present paper have been run to $t \geq 900(a/c_s)$. The necessity of such long-time simulation is clearly illustrated in Fig. 5, where a slow relaxation of the time-averaged χ_i to the asymptotic level is clearly observed. In contrast, data for the largest simulation in Ref. 7 is available only up

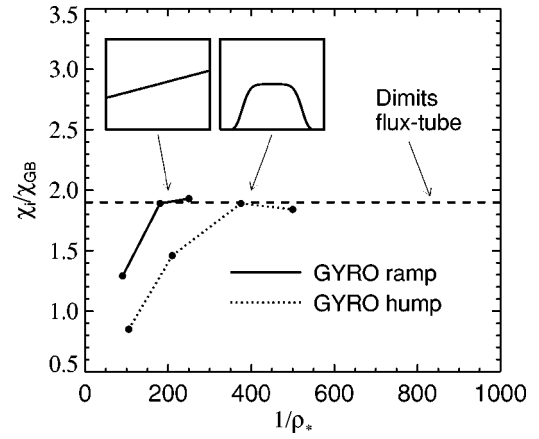


FIG. 4. Comparison of the GYRO data for the GTC *hump* profile (dotted curve) defined in Eq. (1), with a GYRO simulation of the *ramp* profile (solid curve) defined in Eq. (2). The *hump* results are the same as shown in Fig. 1. Note that the more realistic *ramp* profile exhibits gyro-Bohm scaling at substantially smaller system size.

to $t = 500(a/c_s)$. Given the behavior exhibited in Fig. 5, we believe that running the larger GTC simulations to a longer final time may result in better agreement with the local limit. Because GYRO also has the capability to simulate a flux-tube, we have plotted the result of a long-time ($t = 1000a/c_s$) large-radial-box ($L_r = 256\rho_s$) GYRO flux-tube simulation as a dotted horizontal line in Fig. 5. This is to be compared with the Dimits (dashed line) and GS2 (dotted-dashed line) flux-tube results. Remarkably, all results are within about 5% of one another. Note in Fig. 5 the expanded vertical scale in comparison with Figs. 1 and 4.

In summary, we emphasize:

- (1) χ_i obtained from global simulations are found to agree with the gyro-Bohm flux-tube results for sufficiently small ρ_* , as expected from basic theoretical principles;

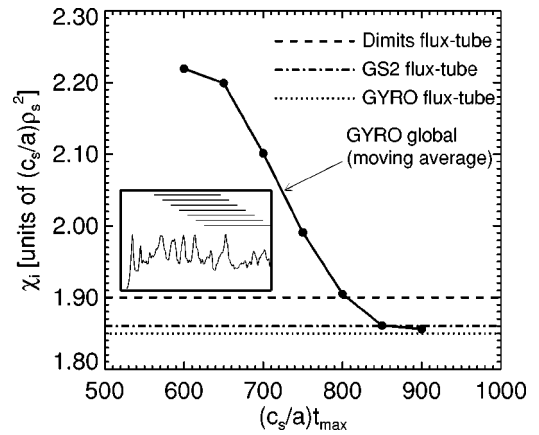


FIG. 5. Time-averaged χ_i from the GYRO global simulation (solid line) at $\rho_* = 1/500$ for the *hump* scenario. The horizontal axis measures the averaging interval: a point at t_{\max} indicates an average over $(c_s/a)t_{\max} - 400 \leq (c_s/a)t \leq (c_s/a)t_{\max}$. Also, three horizontal lines show the final result from flux-tube calculations: Dimits (Ref. 6) (dashed), GS2 (dotted-dashed), and GYRO (dotted). The GYRO flux-tube result was averaged over $500 \leq (c_s/a)t \leq 900$. Plot-in-plot shows the instantaneous χ_i over $0 \leq (c_s/a)t \leq 900$, including horizontal bars which denote averaging windows.

- (2) The rate of approach to the gyro-Bohm limit with decreasing ρ_* depends on the extent to which local growth rates exceed profile shearing rates. This has been discussed in detail in Ref. 1;
- (3) ρ_* -plots such as Fig. 1 are not universal, but in fact highly dependent on the actual profiles (as demonstrated in Fig. 4), $\mathbf{E} \times \mathbf{B}$ shear rates, as well as on nonadiabatic electron physics and plasma shaping.^{1,14}

ACKNOWLEDGMENTS

This work was supported by U.S. DOE Grants Nos. DE-FG03-95ER54309 and DE-FG03-95ER54197.

- ¹R. E. Waltz, J. Candy, and M. N. Rosenbluth, Phys. Plasmas **9**, 1938 (2002).
²J. Candy and R. E. Waltz, J. Comput. Phys. **186**, 545 (2003).
³Z. Lin, S. Ethier, T. S. Hahm, and W. M. Tang, Phys. Rev. Lett. **88**, 195004 (2002).

- ⁴F. Jenko and W. Dorland, Plasma Phys. Controlled Fusion **43**, A141 (2001).
⁵F. Filbet and E. Sonnendrücker, Comput. Phys. Commun. **150**, 247 (2003).
⁶A. M. Dimits, G. Bateman, M. A. Beer, B. I. Cohen, W. Dorland, G. W. Hammett, C. Kim, J. E. Kinsey, M. Kotschenreuther, A. H. Kritiz, L. L. Lao, J. Mandrekas, W. M. Nevins, S. E. Parker, A. J. Redd, D. E. Shumaker, R. Sydora, and J. Weiland, Phys. Plasmas **7**, 969 (2000).
⁷Z. Lin, T. S. Hahm, S. Ethier, W. W. Lee, J. Lewandowski, G. Rewoldt, W. M. Tang, W. X. Wang, L. Chen, and P. H. Diamond, in *Proceedings of Invited Papers, 19th International Conference on Fusion Energy*, Lyon, 2002 (IAEA, Vienna, 2003), TH/1-1.
⁸W. Dorland, F. Jenko, M. Kotschenreuther, and B. N. Rogers, Phys. Rev. Lett. **85**, 5579 (2000).
⁹S. Brunner, M. Fivaz, T. M. Tran, and J. Vaclavio, Phys. Plasmas **5**, 3929 (1998).
¹⁰Z. Lin, T. S. Hahm, W. W. Lee, W. M. Tang, and R. B. White, Science **281**, 1835 (1998).
¹¹Z. Lin, T. S. Hahm, W. W. Lee, W. M. Tang, and P. H. Diamond, Phys. Rev. Lett. **83**, 3645 (1999).
¹²Y. Idomura, S. Tokuda, and Y. Kishimoto, New J. Phys. **4**, 101.1 (2002).
¹³Y. Idomura, S. Tokuda, and Y. Kishimoto, Nucl. Fusion **43**, 234 (2003).
¹⁴J. Candy and R. E. Waltz, Phys. Rev. Lett. **91**, 045001 (2003).